

**UNIVERSIDAD SAN FRANCISCO DE QUITO USFQ**

**Colegio de Ciencias e Ingenierías**

**Control of Power Flux of A Renewable Generation System Using  
A DC-DC Buck-Boost Four Port Converter**

**Danny Stephen Valencia Aguirre**

**Ingeniería Electrónica**

Trabajo de fin de carrera presentado como requisito  
para la obtención del título de  
Ingeniero Electrónico

Quito, 30 de diciembre de 2021

# **UNIVERSIDAD SAN FRANCISCO DE QUITO USFQ**

**Colegio de Ciencias e Ingenierías**

## **HOJA DE CALIFICACIÓN DE TRABAJO DE FIN DE CARRERA**

**Control of Power Flux of A Renewable Generation System Using A DC-DC  
Buck-Boost Four Port Converter**

**Danny Stephen Valencia Aguirre**

**Nombre del profesor, Título académico**

**Nataly Pozo, M.Sc.**

**Alberto Sánchez, PhD.**

Quito, 30 de diciembre de 2021

## © DERECHOS DE AUTOR

Por medio del presente documento certifico que he leído todas las Políticas y Manuales de la Universidad San Francisco de Quito USFQ, incluyendo la Política de Propiedad Intelectual USFQ, y estoy de acuerdo con su contenido, por lo que los derechos de propiedad intelectual del presente trabajo quedan sujetos a lo dispuesto en esas Políticas.

Asimismo, autorizo a la USFQ para que realice la digitalización y publicación de este trabajo en el repositorio virtual, de conformidad a lo dispuesto en la Ley Orgánica de Educación Superior del Ecuador.

Nombres y apellidos: Danny Stephen Valencia Aguirre

Código: 00202186

Cédula de identidad: 1726295353

Lugar y fecha: Quito, 30 de diciembre de 2021

## **ACLARACIÓN PARA PUBLICACIÓN**

**Nota:** El presente trabajo, en su totalidad o cualquiera de sus partes, no debe ser considerado como una publicación, incluso a pesar de estar disponible sin restricciones a través de un repositorio institucional. Esta declaración se alinea con las prácticas y recomendaciones presentadas por el Committee on Publication Ethics COPE descritas por Barbour et al. (2017) Discussion document on best practice for issues around theses publishing, disponible en <http://bit.ly/COPETHeses>.

## **UNPUBLISHED DOCUMENT**

**Note:** The following capstone project is available through Universidad San Francisco de Quito USFQ institutional repository. Nonetheless, this project – in whole or in part – should not be considered a publication. This statement follows the recommendations presented by the Committee on Publication Ethics COPE described by Barbour et al. (2017) Discussion document on best practice for issues around theses publishing available on <http://bit.ly/COPETHeses>.

## RESUMEN

Este trabajo presenta el control del flujo de potencia de un sistema de energía renovable usando un convertor multipuerto DC-DC reductor - elevador de cuatro puertos (BBFPC). El sistema se diseñó considerando el perfil de irradiación de Cumbayá – Ecuador. El BBFPC dispone de dos paneles solares, una batería y una carga resistiva. Se utiliza la modulación por desplazamiento de fase y ancho de pulso para regular el voltaje de salida. El control supervisorio se utiliza para cambiar entre los diferentes modos de operación del sistema: Modo Perturbador y Observador MPPT, Modo de carga de la batería usando el controlador de lógica difusa y el modo de descarga de la batería usando controladores PID. El trabajo presenta y analiza los resultados obtenidos mediante simulación.

**Palabras clave:** Control Difuso, Control Supervisorio, Convertor de Cuatro Puertos, Convertor Multipuerto, Reductor-Elevador.

## ABSTRACT

This work presents the Control of Power Flux of a Renewable Energy System using a DC-DC Buck-Boost Four Port Converter (BBFPC). The system was designed considering an irradiation profile from Cumbayá-Ecuador. BBFPC manages two Solar Panel Arrays, a Battery, and a Resistive load. Phase Shifted - Pulse Width Modulation is used to regulate the output voltage. A supervisory control is used to switch among different operation modes of the system: Perturb and Observe MPPT mode, battery charging mode using Fuzzy Control and battery discharging mode using PID controllers. The paper presents and discusses results performed by simulation.

**Key words:** Buck Boost, Four Port Converter, Fuzzy Control, Multiport Converter, Supervisory Control.

## TABLE OF CONTENTS

I. INTRODUCTION .....	11
II. THEORETICAL FRAMEWORK .....	13
A. DC-DC Buck-Boost Four Port Converter .....	13
B. Operation Analysis of the Buck- Boost Four Port Converter .....	13
III. PROPOSED SYSTEM .....	17
A. Power MosFET .....	17
B. Battery .....	17
C. Solar Panel Arrays.....	18
D. Inductors Design .....	19
E. Blocking Capacitor .....	19
F. Transformer .....	19
G. Rectifier.....	19
H. Load and Filter .....	20
IV. CONTROL SCHEME OF BBFPC.....	21
A. Operation Modes of the System.....	21
B. Supervisory Control .....	23
C. Maximum Power Point Tracking Algorithm .....	23
D. Battery Charging Process.....	23
E. Battery Discharging Process.....	24
V. SIMULATION RESULTS .....	25
VI. CONCLUSIONS .....	30
BIBLIOGRAPHIC REFERENCES .....	31

**INDEX OF TABLES**

Table I. MosFET .....	17
Table II. Battery Specifications .....	17
Table III. Solar Panels Specifications .....	18
Table IV. Fuzzy Rules. ....	24

## INDEX OF FIGURES

Figure 1: BBFPC topology .....	13
Figure 2: Proposed Buck Boost Four Converter.....	14
Figure 3: Modulation Scheme and BBFPC wave-forms .....	16
Figure 4: Control Block Diagram .....	21
Figure 5: Cumbayá Average hourly irradiance profile monthly and annually .....	22
Figure 6: Operation Modes. ....	22
Figure 7: Supervisory Control Flow Chart. ....	25
Figure 8: Total PV1 + PV2 Power and Load Power.....	26
Figure 9: Panels Measurements. ....	27
Figure 10: PV1 Power, PV2 Power, Load Power, Battery Power.....	27
Figure 11: Modulation Scheme, $V_{ab}$ , Inductor 1 Current ( $I_{L1}$ ), Inductor 2 Current ( $I_{L2}$ ), Primary Current ( $I_p$ ) and Load Current ( $I_L$ ). ....	28
Figure 12: Battery SOC, Current and Voltage measurements.....	29

**NOMENCLATURE**

BBFPC	Buck-Boost Four Port Converter
BESS	Battery Energy Storage System
FBC	Full Bridge Converter
GSA	Global Solar Atlas
MPC	Multiport Converter
MPPT	Maximum Power Point Tracking
P&O	Perturb and Observe
PSM	Phased Shifted Modulation
PV	Photovoltaic
PWM	PulseWidth Modulation
RES	Renewable Energy Sources

## I. INTRODUCTION

There is a notable increase of using Renewable Energy in last year, meanwhile fuel consumption has declined [1]. Renewable Energy Sources (RES) such as photo-voltaic, wind, fuel cell, and other Energy Storage technologies experience intermittency in power generation. However, they play a key role in the future to decarbonize the power sector as an essential part of a stand-alone power system supply [2]. To interface an Energy Storage System into a Renewable Energy System, power electronic converters are required. Various topologies of power electronics converters have been proposed over the years [3]. Nonetheless, Multiport Converters (MPC) topologies have become important because they can interface several renewable power sources, such as multi-channel PV panels, hybrid PV, wind turbines, and storage systems at the same time [4].

Traditional DC-link converter topologies are easier to control, since they handle fewer active power switches. Nevertheless, one of the advantages of Multiport Converters is their ability to extend the number of ports according to the application up to N-ports [5]. There are three types of Multiport Converters depending on the topology: fully isolated, fully non-isolated and partly isolated. Some of them are based on DC-DC converters such as: Buck - Boost, Sepik, CUK, among others [6]. For this case of study, a Buck-Boost Four Port Converter (BBFPC) topology is chosen, which has: one isolated unidirectional load port, two non-isolated PV ports, and one non-isolated bidirectional battery port [6].

The focus of this work is to control the power flux of the whole system, maintaining the constant supply of energy to the load according to its requirements, regardless of the variations of the renewable resource. Considering that emerging high-speed Silicon Carbide (SiC) and Gallium Nitride (GaN) power semiconductor devices offer significant design and performance-based benefits over common MosFET devices [7]. Also, these devices improve

power conversion systems efficiency. The system proposed uses High Speed MosFET with a switching frequency of 100 [kHz].

To control the system, three operating modes are established according to load requirements and solar irradiation profiles. The data are selected from the Global Solar Atlas or “GSA” in a specific location of Cumbayá – Ecuador. Moreover, the algorithm of Maximum Power Point Tracking used for extracting maximum power from PV arrays is Perturb and Observe (P&O). The control techniques applied for charging and discharging battery are Fuzzy Logic Controller and PID Controller respectively. Pulse Width Modulation (PWM) Technique and Phased Shifted Modulation (PSM) is used to control the Buck-Boost Four Port Converter.

This paper is divided in the following sections. In section II, the DC-DC Buck- Boost Four Port Converter is analyzed, as well as its principle of operation and modulation scheme. In section III, the proposed system is described considering important design aspects. In section IV, the proposed control system scheme is developed. In section V, simulation results and performance of the BBFPC is presented. Finally, in section VI, conclusions are given.

## II. THEORETICAL FRAMEWORK

### A. DC-DC Buck-Boost Four Port Converter

This topology combines two Bidirectional DC-DC converters. In Figure 1 is depicted the BBFBC, where it can be seen three sources called V1, V2, and V3. Each power source can deliver power to the load. Additionally, V2 and V3 sources can feed V1. Hence, three ports are non-isolated, and the load port is isolated by a transformer. This feature represents an advantage, because power flux in each port can be controlled by a modulation scheme, which will be described below [6].

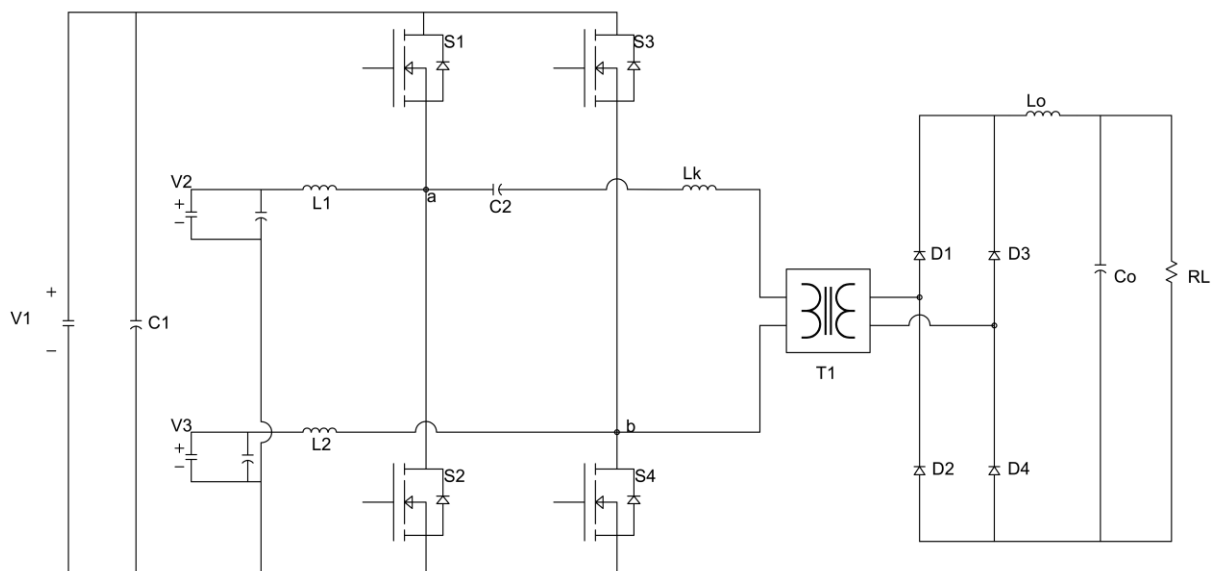


Figure 1: BBFPC topology

### B. Operation Analysis of the Buck- Boost Four Port Converter

In this case of study, BBFPC manages two Solar Panels Arrays, a BESS, and a resistive load. As can be seen in Figure 2, the BBFPC has four power switches S1, S2, S3, and S4 that operate in a complementary state for each leg. Also, the first leg is similar to a boost converter in which S1 and S2 connect with Solar Panel Array 1 (PV1) and the battery through Inductor 1 (L1). On the other hand, the second leg contains S3 and S4 that interface Solar Panel Array

2 (PV2) with the battery through Inductor 2 (L2). Moreover, power transfer of PV1, PV2 and the battery are controlled by duty cycle  $\delta_1$ , and  $\delta_2$  of each leg, respectively. The Full-Bridge Converter (FBC) is formed by D1, D2, D3, D4, which rectifies the voltage in the secondary side. Besides, an LC filter smooths the Load Voltage (VL) and Current Load (ILO).

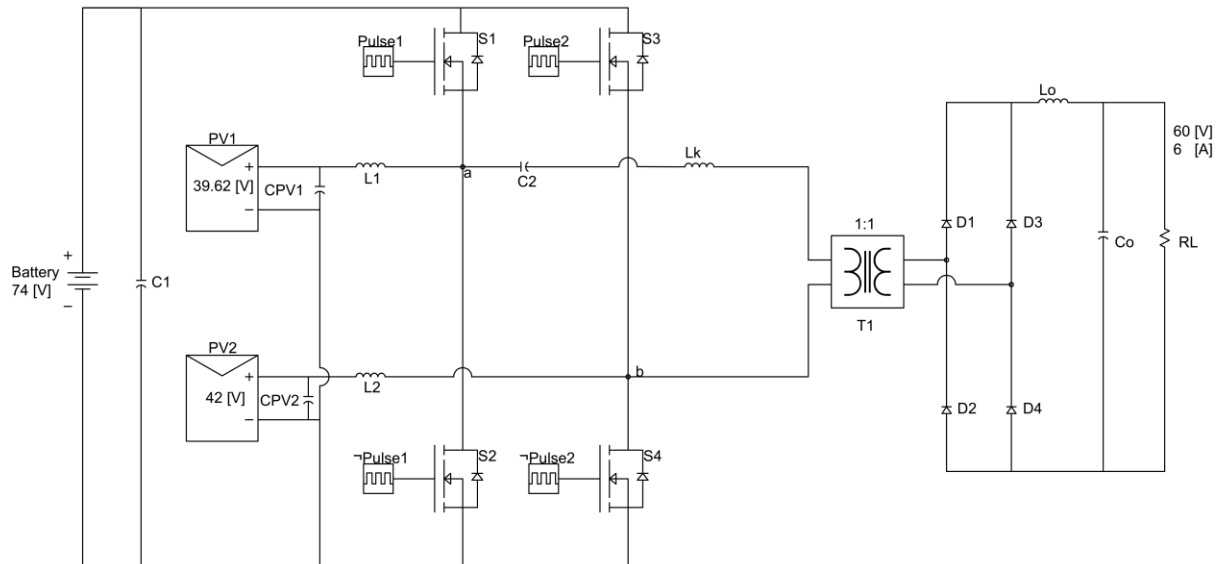


Figure 2: Proposed Buck Boost Four Converter

The square-wave voltages of each switching leg  $V_a$  and  $V_b$  are Phased Shifted by the  $\phi$  angle. Additionally, it controls the voltage at the primary side of the transformer  $V_{ab}$ . As a result, each leg of power switches form a boost converter, which conversion voltage is defined by the following equations [6]:

$$VB = \frac{VPV1}{1 - \delta_1} = \frac{VPV2}{1 - \delta_2} \quad (1)$$

$$\begin{cases} VPV1 = (1 - \delta_1)VB \\ VPV2 = (1 - \delta_2)VB \end{cases} \quad (2)$$

In equation 2  $VB$  is the Battery Voltage,  $VPV1$  and  $VPV2$  are the Voltage of Solar Panel Array 1 and 2, respectively. Likewise, Duty Cycle of leg 1 and 2 are called  $\delta_1$ , and  $\delta_2$ . Therefore, the calculation for the Load Voltage ( $V_L$ ) is in the following equation [6]:

$$V_L = \begin{cases} nVB \left[ \frac{\phi}{\pi} (1 - \Delta\delta_{21}) + 2\Delta\delta_{21} - 2\Delta\delta_{21}^2 \right], & \Delta\delta_{21} > 0 \\ nVB \left[ \frac{\phi}{\pi} (1 + \Delta\delta_{21}) \right], & \Delta\delta_{21} < 0 \end{cases} \quad (3)$$

Where, the number of turns of the transformer is  $n$ . Also, the relation of  $\delta_{21} = \delta_2 - \delta_1$ . Thus, there are two main conditions  $\delta_{21}$  greater than zero and  $\delta_{21}$  lower than zero. According to these equations,  $\delta_1$  and  $\delta_2$  are used to control power flux between Solar Panel Arrays and BESS, and  $\phi$  angle is used to regulate the voltage  $V_{ab}$ . Therefore, some constraints must be met to control the output variable  $V_L$ . The restrictions are shown below [6]:

$$\begin{cases} \frac{\phi}{2\pi} \leq \delta_1 \\ \frac{\phi}{2\pi} \leq 1 - \delta_2 \end{cases} \quad (4)$$

$$\frac{\phi}{2\pi} \leq \delta_1 \text{ and } \frac{\phi}{2\pi} \leq 1 - \delta_2 \quad (5)$$

The modulation scheme in Figure 3 is based on the key waveforms presented in [6]. It shows the Phase Shifted - Pulse Width Modulation generation. It occurs at the crossover of the reference deltas and the saw-tooth. Further, the phase shift between each saw-tooth is controlled by the angle  $\phi$ . For this MPC, the modulation scheme has six switching states described following:

- *Switching State I:* This state occurs between times  $t_0$  and  $t_1$ . Therefore, S2 and S3 are ON. Inductor 1 is charging and Inductor 2 is discharging. The secondary side of the transformer is short circuit by diodes D1 to D4 because they are supplied by the current  $I_{Lo}$ .
- *Switching State II:* This state goes from  $t_1$  to  $t_2$ . In this state, S2 and S3 remain ON to supply the load. D2 and D3 are forward biased.

- *Switching State III:* In  $t_2 - t_3$ , Power Switches S2, and S4 are ON, the Inductor Current 1 (IL1) remains increasing and Inductor Current 2 (IL2) starts to grow as well. Diodes D2 and D3 are forward biased.
- *Switching State IV:* This state happens between times  $t_3$  and  $t_4$ . S1 and S4 are ON, thus Inductor Current 1 (IL1) begins to decrease and Inductor Current 2 (IL2) is still charged. Also, Output Inductor Current (ILo) is freewheel through diodes D1 to D4.
- *Switching State V:* In Switching State V, from  $t_4$  to  $t_5$ , power switches S1 and S4 are ON, D1 and D4 are ON as well, thus the load is supplied by power sources.
- *Switching State VI:* Finally, at  $t_5 - t_6$ , S1 and S3 are ON. Output Inductor Current (ILo) is flowing through diodes D1 to D4. Inductor Current 1 (IL1) and Inductor Current 2 (IL2) are decreasing.

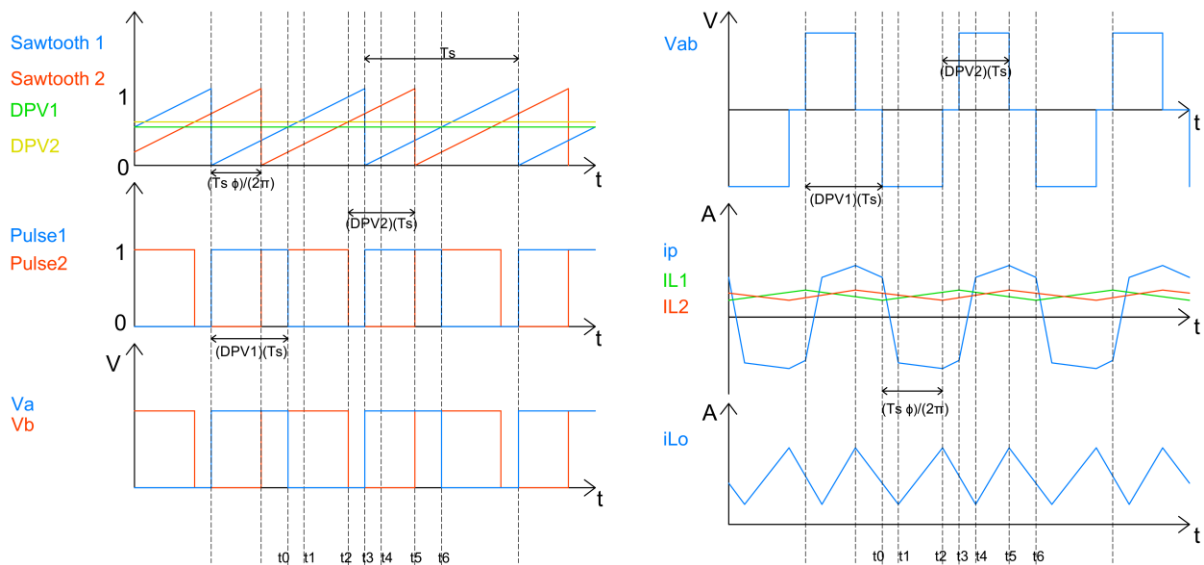


Figure 3: Modulation Scheme and BBFPC wave-forms [6].

### III. PROPOSED SYSTEM

This section shows the design aspects of the proposed BBFPC. The Renewable System is shown in Figure 2. It is designed considering the irradiation profiles taken from the Global Solar Atlas in Cumbayá - Ecuador. The following subsections show important design aspects of the DC-DC BBFPC components:

#### A. Power MosFET

The devices chosen for both legs of the BBFPC are high switching frequency MosFETs. The Switching Frequency ( $f_s$ ) is 100[kHz]. The main parameters are shown in Table I.

Table I. MosFET [8].

Device	Parameter	Value
MosFET [100KHz]	Ron	45 [mΩ]
	Lon	30[nH]
	Rd	4 [Ω]
	Vf	4.60 [V]
	Rs	100 [kΩ]

#### B. Battery

Table II. Battery Specifications [9].

Device	Parameter	Value
Lithium - Ion Battery	Nominal Voltage	74[V ]
	Rated Capacity	20[Ah]
	Battery response time	550[ms]
	Maximum Capacity	20[Ah]
	Cutt-off Voltage	55.50[V ]
	Fully Charged voltage	86.135[V ]
	Nominal Discharge Current	8.6957[A]
	Internal Resistance	77[mΩ]
	Capacity at nominal Voltage	18.087[Ah]
	Exponential Zone [V Ah]	[79.9486 0.982609]
	Discharge Current [i1,i2,i3][A]	[6.5 13 32.5]

To choose an adequate device, it is important to consider the amount of time during a day that the BESS is charging and discharging. Therefore, it must be selected considering a power balance between the State of Charge and the State of Discharge. Thus, no matter irradiation changes during the day it has to be able to supply the load requirements. Therefore, the selection of a battery with the mentioned features are summarized in Table.II.

### C. Solar Panel Arrays

Due to the boost topology performance of the BBFPC legs, Solar Panel arrays must generate a lower voltage than the Battery (VB). Moreover, for this application, two Solar Panels are connected in parallel considering the sort for the system autonomy. The main features are presented in Table.III.

*Table III. Solar Panels Specifications [10], [11].*

<b>Device</b>	<b>Parameter</b>	<b>Value</b>
Solar Panel 1	Power_max	370[W]
	Voc	47.33[V ]
	Vmp	Vmp 39.51[V ]
	Voc (%/deg.C)	-0.29
	Ncell	60
	Isc	9.77[A]
	Imp	9.37[A]
	Isc (%/deg.C)	0.05
	Performance%	20.51%
Solar Panel 2	Power_max	530[W]
	Voc	49.54[V ]
	Vmp	42[V ]
	Voc (%/deg.C)	-0.35
	Ncell	60
	Isc	13.34[A]
	Imp	12.62[A]
	Isc (%/deg.C)	0.06
	Performance%	21.66%

### D. Inductors Design

Inductor 1 (L1) and Inductor 2 (L2) must have the same value to maintain a current balance in the BBFPC. Regarding Equation 6 [12],  $L1 = L2 = 72[\mu\text{H}]$ :

$$L1 = L2 = \frac{VB(1 - \delta)}{\Delta IL1 f_s} \quad (6)$$

### E. Blocking Capacitor

The blocking capacitor (C2) is chosen considering an asymmetrical operation of the BBFPC's switching legs. Therefore, the voltage of C2 depends on Equation 7 [12]. Specifically, the value chosen for this case of study is  $C2=15[\mu\text{F}]$ .

$$V_{C2} = V B \left[ \left( \delta 2 + \frac{\phi}{2\pi} - \delta 1 \right) - \frac{\phi}{2\pi} \right] \quad (7)$$

### F. Transformer

An ideal transformer is chosen with a number of turns (n) ratio equal to 1:1. However, for simulation purposes, a resistor  $R_t$  of  $1[\text{M}\Omega]$  was added in parallel to the transformer. Moreover, the Leakage Inductor (Lk) has a typical transformer value of  $0.45[\mu\text{H}]$  [13]. Nevertheless, the maximum leakage value can be calculated by Equation 8 [12], where PL is the power delivered to the load:

$$Lk = \left( \frac{n^2 VL^2}{4f_s PL} \right) \left( \frac{2 \delta_{max} VB}{n 2\pi VL} - 1 \right) \quad (8)$$

### G. Rectifier

A Full-Wave Bridge Rectifier is connected to the secondary side of the transformer to deliver DC current to the load. It is important to note that current flows through diodes pairs

D1 and D4 as well as D2 and D3 depending on the switching state. Moreover, diodes D1 - D4 have ideal parameters.

### **H. Load and Filter**

This case of study considers a load represented by  $R_L = 10[\Omega]$ . Moreover, in nominal conditions, the load will consume 6 [A] and 60 [V]. As a result, Load Power (PL) consumption is approximately 360 [W]. Besides, the LC load filter is designed for a current ripple of 10% of nominal load current, and a voltage ripple of 5% of nominal load voltage. The values for this system are  $L_o = 83.33[\mu\text{H}]$  and  $C_o = 130.46[\mu\text{F}][12]$ .

#### IV. CONTROL SCHEME OF BBFPC

In Figure 4, the Control Block Diagram of the whole system is presented. The following subsections describe the main points of the power flux control of the BBFPC.

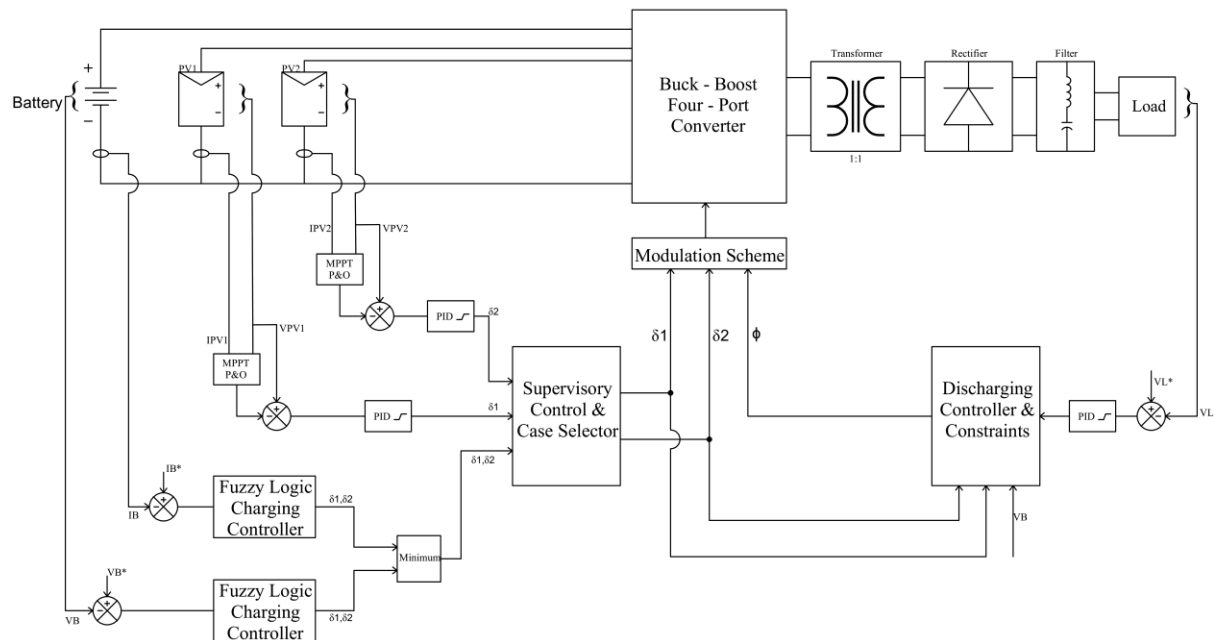


Figure 4: Control Block Diagram

##### A. Operation Modes of the System

The system is conditioned by the amount of solar irradiation available. The Figure 5 displays the average hourly irradiation profile per month during a whole year, in Cumbayá, Quito - Ecuador. Moreover, the profile used for the simulations is in light blue and it represents the average solar irradiation obtained in a year.

Subsequently, Figure 6 indicates each operation mode of the system separated by vertical green lines. This case of study contemplates 3 modes of operation. The system prioritizes feeding the load through the Solar Panel Arrays and battery. It is important to consider the SOC to manage the battery performance. The operation modes are described below:

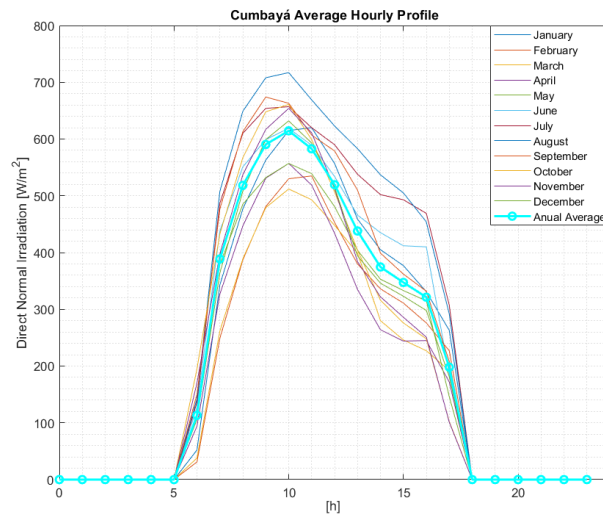


Figure 5: Cumbayá Average hourly irradiance profile monthly and annually [14].

- *Mode A*: The power of the Solar Panels Arrays is lower than the minimum power due to the solar irradiation being close to zero. Therefore, only the battery supplies power to the load.
- *Mode B*: The power of Solar Panel Arrays is not enough to supply the load. Thus, battery and PV supply power to the load. In this case-scenario, PV works under the Perturb and Observe MPPT algorithm.
- *Mode C*: The power of Solar Panel Arrays is greater than the power demanded by the load. Therefore, PV supplies the load and charges the battery.

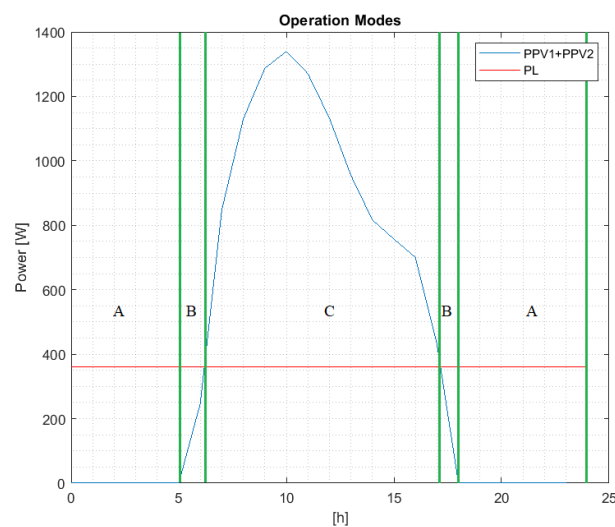


Figure 6: Operation Modes.

## **B. Supervisory Control**

Full control of the system is based on the operation modes mentioned above. In addition, Figure 4 presents the proposed control block diagram of the system. Supervisory Control measures the voltage and current of each device such as Battery, PV1, PV2, and Load. Then, all the obtained values are used to calculate Battery Power, PV Power, and Load Power. Finally, power values and battery SOC are compared to select the system operation mode. The conditions for the correct operation of the system are illustrated in the flowchart in Figure 7. Finally, Supervisory Control determines the control variables that will be used by the case selector to identify each operation mode.

## **C. Maximum Power Point Tracking Algorithm**

For this case of study, the P&O MPPT algorithm is performed during operation mode B. It should be noted that this algorithm takes the voltage and current measurements to calculate the power. Then, the calculated power value and voltage measurement are compared with the previous data. Thus, the algorithm determines if it is required to increase or decrease the output voltage reference [15]. As a result, the proposed system will take this reference to calculate the error. Consequently, it is the input for the PID controller that determines the respective  $\delta 1$  and  $\delta 2$  for PV1 and PV2 respectively. It is important to mention that small increments in the algorithm will help to keep the system stable when the panel operating conditions change [15].

## **D. Battery Charging Process**

The surplus power during operation mode C is used to charge the battery and supply the load. A Fuzzy Logic Controller (FLC) is used for Battery Charging Process. This control technique does not require the transfer function of the system, which is an advantage for processes in which quantitative techniques require a complicated analysis [16], [17]. The

voltage and current Fuzzy Logic Controllers designed for the system has the following characteristics:

- The error and error variation are the inputs of FLC.
- The membership functions have a triangular shape.
- The fuzzification stage has five fuzzy sets distributed in a range. The fuzzy sets are: Negative Big (NB), Negative Small (NS), Zero (Z), Positive Small (PS) and Positive Big (PB).
- Bisector method is used in the defuzzification process. It calculates the weight of each triangular shape membership function based on the average of the centroid volume.
- The rules determine the behavior of the controller and are summarized in Table. IV. They have been programmed according to the behavior of the system. Where, H = High, UM = Upper Middle, M = Middle, L=Low, LM = Low Middle.

*Table IV. Fuzzy Rules.*

<b>de \ e</b>	<b>NB</b>	<b>NS</b>	<b>Z</b>	<b>PS</b>	<b>PB</b>
<b>NB</b>	L	L	L	LM	M
<b>NS</b>	L	L	LM	M	UM
<b>Z</b>	L	LM	M	UM	H
<b>PS</b>	LM	M	UM	H	H
<b>PB</b>	M	UM	H	H	H

### **E. Battery Discharging Process**

Battery Discharging Process contemplates the operation modes A and B. When the battery is discharging, the among of power that the load requires is sent to the secondary side of the transformer using the BBFPC. To maintain a constant voltage  $V_{ab}$  in the load side, a Proportional-Integral-Derivative (PID) control was developed and tuned. These controllers calculate the correct value of  $\phi$  angle, considering the restrictions presented in Equation 4.

## V. SIMULATION RESULTS

In this section, the results of the simulations performed in the Matlab-Simulink software are presented. There are some important testing conditions for the correct operation. For example, the sampling time of the simulation  $t_m = 0.1[\mu s]$ , was chosen to have enough points per period, since the system works at a switching frequency of 100 [kHz]. Therefore, the computational cost becomes evident due to the large amount of calculations and data handled by the proposed scheme. For this reason, the original irradiation profiles are scaled to a time of 0.0024 [s].

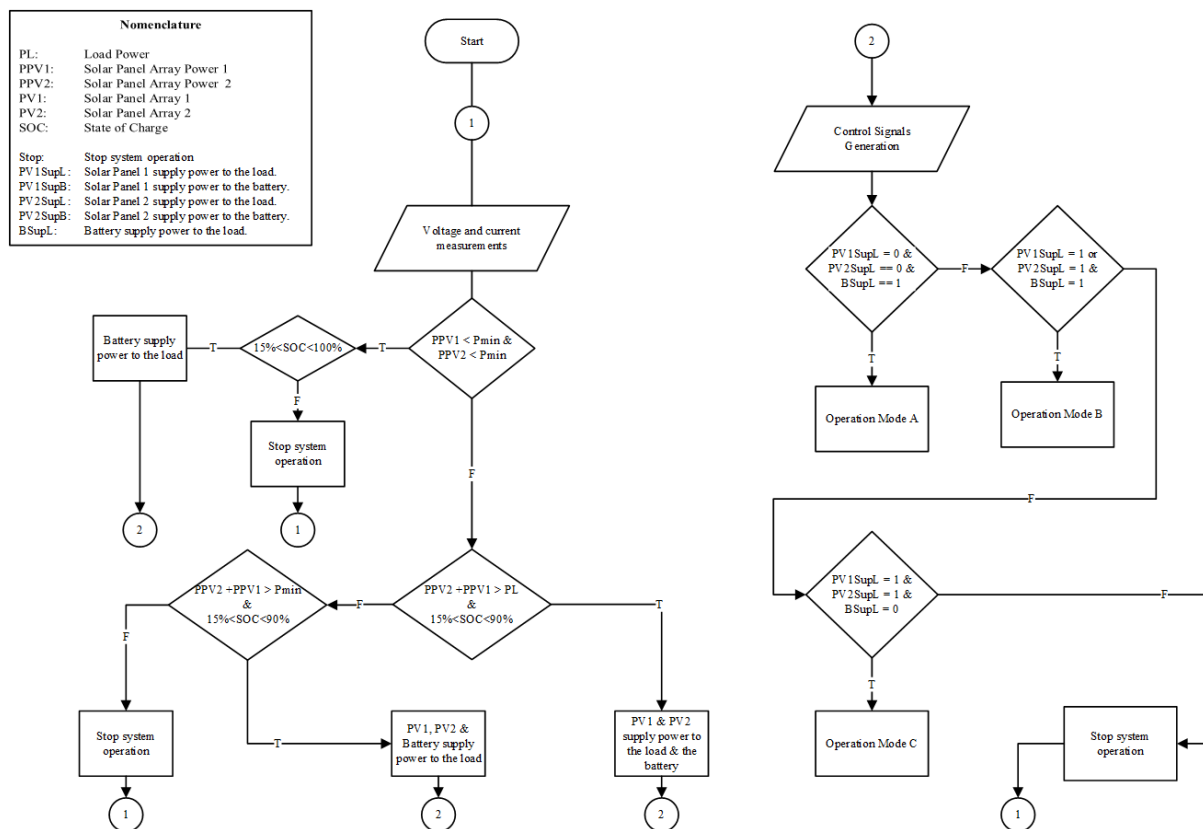
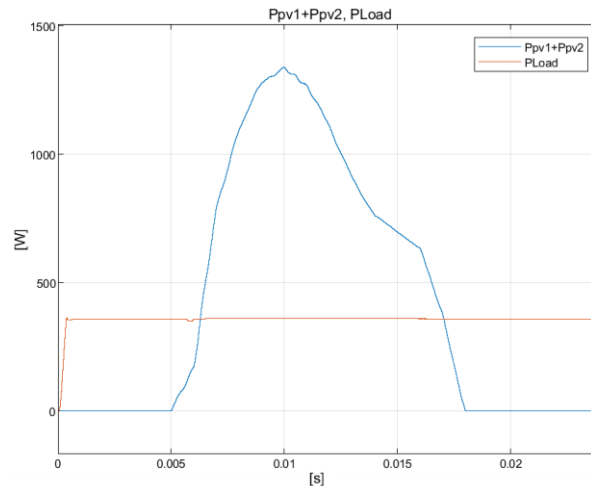


Figure 7: Supervisory Control Flow Chart.

System operation conditions the curves in Figure 8. Indeed, they are similar to the waveforms presented in Figure 6. However, a distinction is made between the operation modes in which the system works. On one hand, the power of the load is almost constant during the whole profile at around 360[W].



*Figure 8: Total PV1 + PV2 Power and Load Power.*

On the other hand, voltages, currents, solar irradiation, and temperature of PV1 and PV2 are displayed in Figure 9. It is important to mention that both panels receive the same irradiation profile. This case of study considers that the renewable power sources will be installed at the same place. Likewise, it is observed that the temperature remains in normal conditions since its variation would imply other considerations that are not part of the focus of this work. Hence, it is observed that the generated power is used as defined in the supervisory control. In brief, solar panels power is used during the irradiation time to supply the load. However, when the power is less than the load demands, the battery continues in discharge mode to contribute energy along with the panels. Also, when there is surplus panels power, they supply the load and battery goes into charging mode.

Regarding the wave-forms shown in Figure 10, negative battery power shows the charging mode that corresponds to the surplus power period. Indeed, the negative sign of Battery Power is due to the measuring instrument and indicates that the battery is charging. It is important to note a transient at the beginning of the simulation results. It occurs due to the initial conditions of the simulation. For instance, the system starts the simulation with zero values at currents and voltages in inductors and capacitors, respectively. In addition, small oscillations can be noticed at the selection of the operation modes.

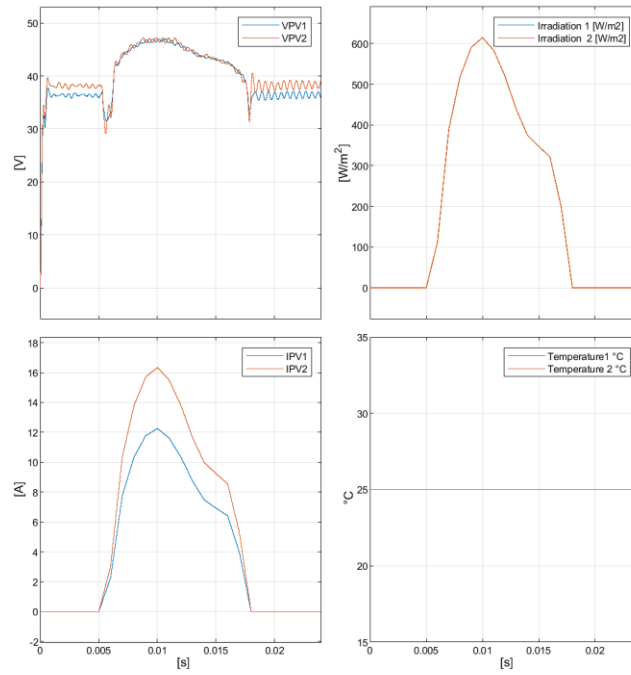


Figure 9: Panels Measurements.

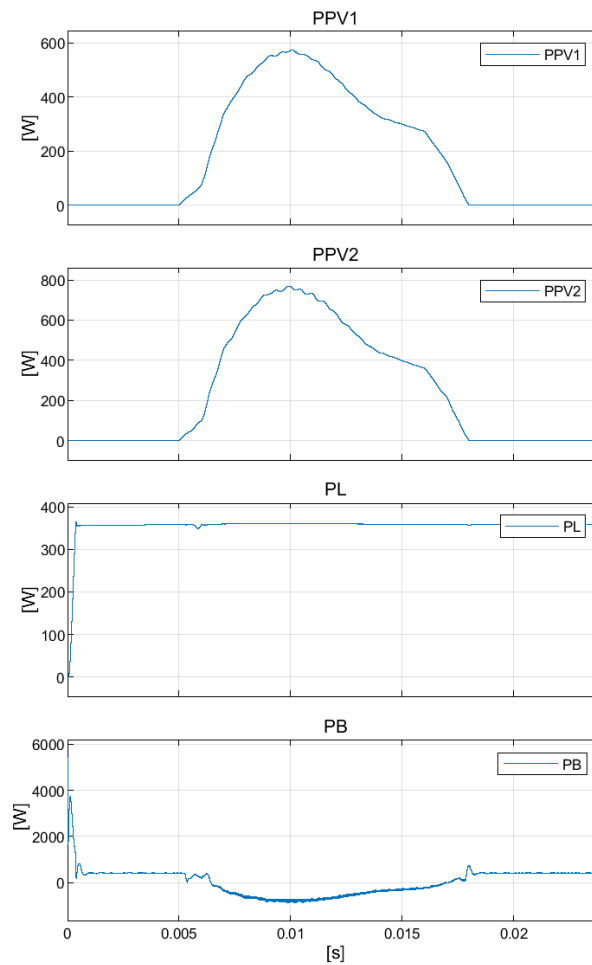
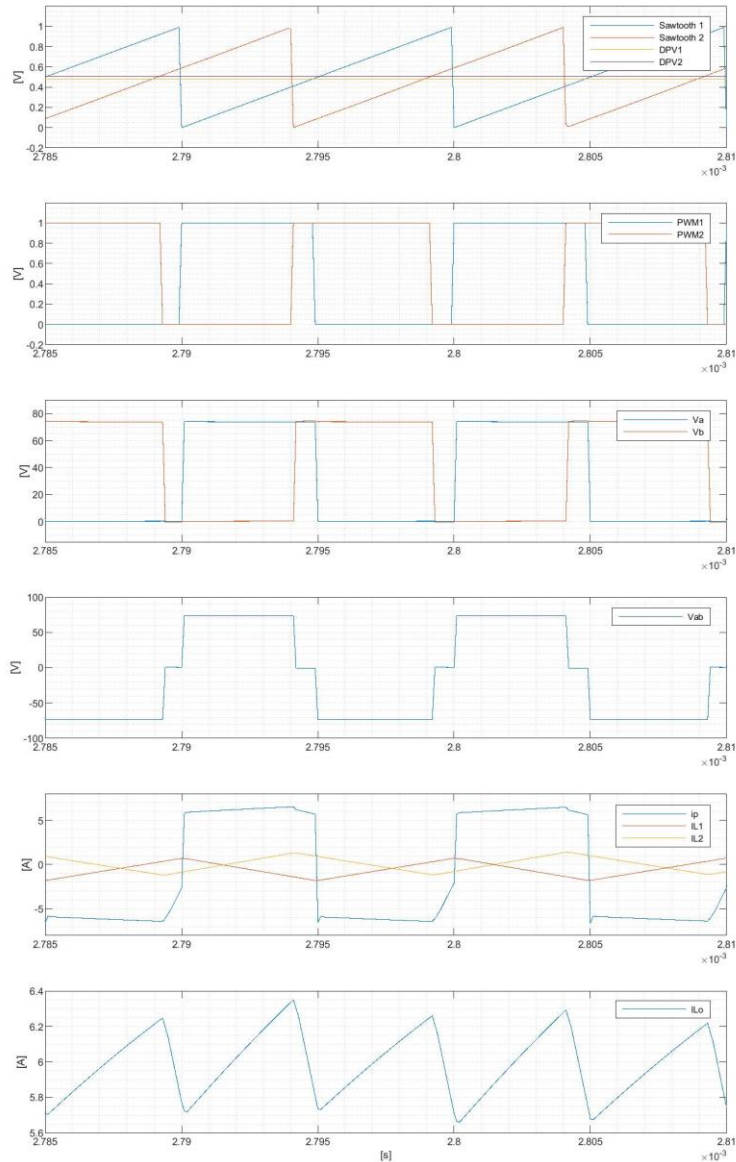


Figure 10: PVI Power, PV2 Power, Load Power, Battery Power.

The measurements depicted in Figure 11 are adjusted to observe in detail two periods of steady state wave-forms. As a result, the modulation scheme presents the switching of the MosFET due to the Phase Shifted Pulse Width Modulation. Consequently, the  $\phi$  angle regulates the voltage at the output of the BBFPC.



*Figure 11: Modulation Scheme,  $V_{ab}$ , Inductor 1 Current ( $IL1$ ), Inductor 2 Current ( $IL2$ ), Primary Current ( $I_p$ ) and Load Current ( $IL$ ).*

In addition, the steady-state current peaks of  $IL1$  and  $IL2$  are in the range of  $[-2, 2]$  [A]. The primary current is 6 [A] with a current ripple of 10%. This current is transferred to the secondary side of the topology. Then, considering the number of turns of the transformer, the

current flows through rectification and filter stages and reaches a DC value of 6 [A] in the load. Indeed, the wave-forms are consistent with the modulation scheme presented in Figure 3.

The battery SOC, current, and voltage are in Figure 12. Thus, its performance indicates periods of charging and discharging according to the amount of power generated by the renewable resource. Discharge Battery mode appears at periods of low irradiation and Charging Battery mode is performed at high irradiation levels, to guarantee the self-sustainability of the system during a full day. Indeed, as mentioned above Figure 12 displays a negative current due to the measuring instrument when the system is operating in Mode C.

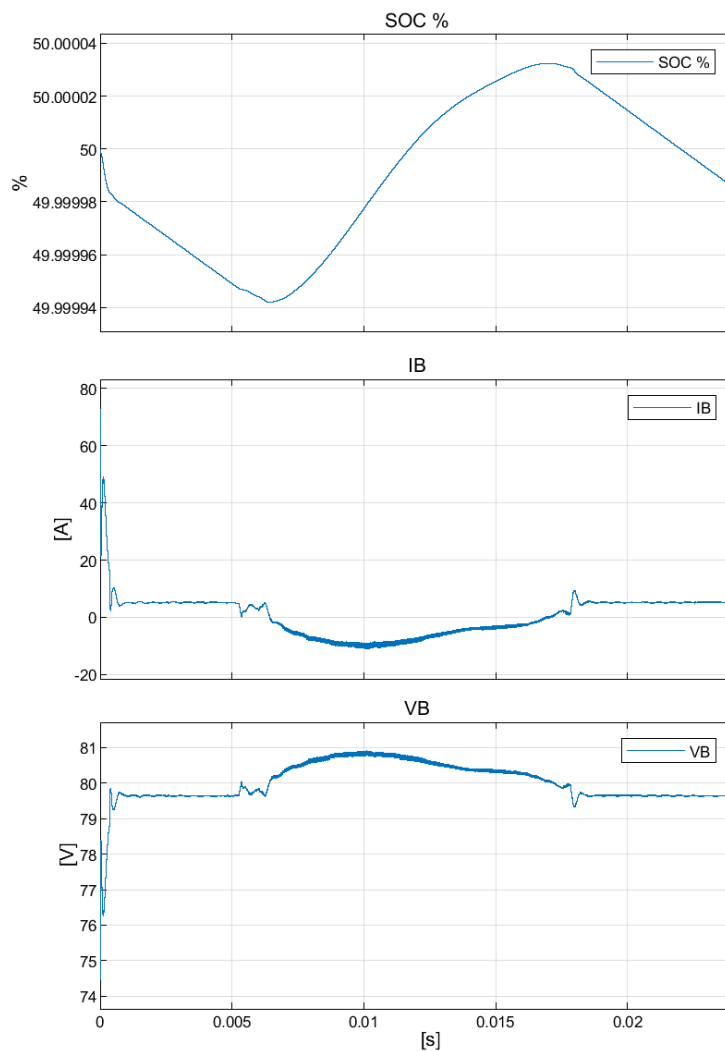


Figure 12: Battery SOC, Current and Voltage measurements.

## VI. CONCLUSIONS

In this paper, a renewable energy system for domestic application was designed considering a DC-DC Buck-Boost Four Port Converter. Then, the proposed scheme controlled the power flux in each port of the designed BBFPC. Also, the PID and Fuzzy Logic controllers' operations were corroborated according to the operating conditions of the system. Finally, the performance in the three operation modes was verified by simulation.

Further simulations are recommended to expand the focus of this case of study. They may include different solar profiles, temperature changes, incremental conductance for MPPT technique, or other renewable energy sources. Also, it is suggested to replace PID's controllers with fuzzy logic, predictive control, robust control, sliding mode control, etc. Consequently, a future implementation will have additional considerations to those presented in the simulations. For instance, commutation dead times, control and power isolation, switching frequency circuitry, drivers for SiC and GaN devices, among others.

**BIBLIOGRAPHIC REFERENCES**

- [1] IEA, “Renewables – global energy review 2021 – analysis,” Apr 2021. [Online]. Available: <https://www.iea.org/reports/global-energy-review-2021/renewables>
- [2] S. Mukherjee, D. Mukherjee, and D. Kastha, “Multiport soft-switching bidirectional dc-dc converter for hybrid energy storage systems,” in 2019 IEEE Applied Power Electronics Conference and Exposition (APEC), 2019, pp. 2103–2109.
- [3] T. Chaudhury and D. Kastha, “A high gain multiport dc–dc converter for integrating energy storage devices to dc microgrid,” IEEE Transactions on Power Electronics, vol. 35, no. 10, pp. 10 501–10 514, 2020.
- [4] Q. Tian, G. Zhou, R. Liu, X. Zhang, and M. Leng, “Topology synthesis of a family of integrated three-port converters for renewable energy system applications,” pp. 5833–5846, 2021.
- [5] Y. Zhang, J. He, and D. M. Ionel, “Modeling and control of a multiport converter based ev charging station with pv and battery,” in 2019 IEEE Transportation Electrification Conference and Expo (ITEC), 2019, pp. 1–5.
- [6] H. Wu, P. Xu, H. Hu, Z. Zhou, and Y. Xing, “Multiport converters based on integration of full-bridge and bidirectional dc–dc topologies for renewable generation systems,” IEEE Transactions on Industrial Electronics, vol. 61, no. 2, pp. 856–869, 2014.
- [7] J. Xu, L. Gu, Z. Ye, S. Kargarrazi, and J. M. Rivas-Davila, “Cascode gan/sic: A wide-bandgap heterogenous power device for high-frequency applications,” IEEE Transactions on Power Electronics, vol. 35, no. 6, pp. 6340–6349, 2020.

- [8] Infineon, “EasyDUAL module with CoolSiC™ Trench MOSFET and PressFIT / NTC,” FF45MR12W1M1\_B11 datasheet, Mar.2020 [Revised Dic.2021].
- [9] Pacto Power Co., “72v 20 Ah Portable Lithium-Ion BATTERY Pack Product Data Sheet,” PPCB-7220 datasheet, Oct. 2020 [Revised Dic. 2021].
- [10] SunDay Energy, “9BB CELL MONOCRYSTALLINE MODULES 370W - 410W,” SDM-375 datasheet, 2021 [Revised Dic.2021].
- [11] RESUN, “RS8I-M(535-560),” RS8I -M(535 -560) datasheet, 2021[RevisedDic.2021].
- [12] W. Li, J. Xiao, Y. Zhao, and X. He, “Pwm plus phase angle shift (ppas) control scheme for combined multiport dc/dc converters,” IEEE Transactions on Power Electronics, vol. 27, no. 3, pp. 1479–1489, 2012.
- [13] Pulse Electronics, “High frequency flat coil planar transformers,” P773.H datasheet, Feb. 2018 [Revised Dic. 2021].
- [14] GSA, “Cumbayá,” 2021. [Online]. Available: <https://globalsolaratlas.info/map?s=-0.201169,-78.429365,10&c=-0.658135,-80.185432,11>
- [15] M. G. Villalva and E. R. F., “Analysis and simulation of the p amp;o mppt algorithm using a linearized pv array model,” in 2009 35th Annual Conference of IEEE Industrial Electronics, 2009, pp. 231–236.
- [16] C. Lee, “Fuzzy logic in control systems: fuzzy logic controller. i,” IEEE Transactions on Systems, Man, and Cybernetics, vol. 20, no. 2, pp. 404– 418, 1990.
- [17] E. Cox, “Fuzzy fundamentals,” IEEE Spectrum, vol. 29, no. 10, pp. 58–61, 1992